Suppressing T cell motility induced by anti–CTLA-4 monotherapy improves antitumor effects

Maria Grazia Ruocco,[1,2] Karsten A. Pilones,[1] Noriko Kawashima,[1] Michael Cammer,[1,2] Julie Huang,[1,2] James S. Babb,[3] Mengling Liu,[4] Silvia C. Formenti,[5] Michael L. Dustin,[1,2] and Sandra Demaria[1]

[1]Department of Pathology, New York University School of Medicine, New York, New York, USA. [2]Program in Molecular Pathogenesis, The Helen L. and Martin S. Kimmel Center for Biology and Medicine at the Skirball Institute for Biomolecular Medicine, New York University Langone Medical Center, New York, New York, USA. [3]Department of Radiology, [4]Department of Environmental Medicine, and [5]Department of Radiation Oncology, New York University School of Medicine, New York, New York, USA.

A promising strategy for cancer immunotherapy is to disrupt key pathways regulating immune tolerance, such as cytotoxic T lymphocyte–associated protein 4 (CTLA-4). However, the determinants of response to anti–CTLA-4 mAb treatment remain incompletely understood. In murine models, anti–CTLA-4 mAbs alone fail to induce effective immune responses to poorly immunogenic tumors but are successful when combined with additional interventions, including local ionizing radiation (IR) therapy. We employed an established model based on control of a mouse carcinoma cell line to study endogenous tumor-infiltrating CD8$^+$ T lymphocytes (TILs) following treatment with the anti–CTLA-4 mAb 9H10. Alone, 9H10 monotherapy reversed the arrest of TILs with carcinoma cells in vivo. In contrast, the combination of 9H10 and IR restored MHC class I–dependent arrest. After implantation, the carcinoma cells had reduced expression of retinoic acid early inducible–1 (RAE-1), a ligand for natural killer cell group 2D (NKG2D) receptor. We found that RAE-1 expression was induced by IR in vivo and that anti-NKG2D mAb blocked the TIL arrest induced by IR/9H10 combination therapy. These results demonstrate that anti–CTLA-4 mAb therapy induces motility of TIL and that NKG2D ligation offsets this effect to enhance TILs arrest and antitumor activity.

Introduction

The presence of tumor-infiltrating lymphocytes (TILs) is predictive for a positive outcome in human cancer (1), but relatively little is known about how TILs interact with tumor components in vivo (2). Our understanding of this process is based on studies using mouse models and two-photon laser scanning microscopy (TPLSM) (3). Studies using the OT-1 model system with K^b-OVA as an antigen in a T lymphoma context and a single study using endogenous TILs in conjunction with vaccination for a viral antigen in a lung carcinoma setting all found that stable TIL–tumor cell interactions are a feature of tumor rejection (2, 4, 5). Recent FDA approval of anti–CTLA-4–based immunotherapies for treatment of melanoma (6) has raised interest in understanding how non-antigen-specific immunotherapies influence the interactions of TILs and tumor cells. However, there are currently no data on such effects in tumors in vivo.

The ability of anti–CTLA-4 mAbs to induce immune-mediated tumor regression and specific T cell memory was first demonstrated in mouse tumor models of relatively immunogenic tumors (7). Significant antitumor activity of anti–CTLA-4 mAbs against poorly immunogenic tumors required combination with additional interventions. Increased priming of antitumor T cells by vaccination and/or other "conditioning" effects of chemotherapy and radiotherapy were a prerequisite for effective anti–CTLA-4 mAb–mediated antitumor immunity in the setting of poorly immunogenic tumors (8–10).

CTLA-4 suppresses immune responses by cell-autonomous and non-autonomous mechanisms. Non-autonomous effects of CTLA-4 include the reduction of CD80 and CD86 from the surface of dentritic cells by regulatory and effector T cell–mediated trogocytosis (11, 12). Cell-autonomous functions of CTLA-4 include competition with CD28 for binding to shared ligands CD80 and CD86 (13–15), engagement of negative signaling pathways (16), inhibition of activating signaling (17, 18), and inhibition of transcriptional programs in CD8$^+$ T cells (19). A single dose of anti–CTLA-4 mAb during priming increases the expansion and effector function of CD8$^+$ T cells (20).

Anti–CTLA-4 mAb is generally thought to block the effect of CTLA-4 interaction with CD80 and CD86; however, it may also activate signaling pathways in T cells. Anti–CTLA-4 mAb triggers antiapoptotic, pro-adhesion, and pro-polarity signals (21–23). Anti–CTLA-4 mAbs enhance T cell motility on ICAM-1–coated surfaces and can override anti-CD3–mediated stop signals in vitro (24). Recent data in different tolerance models also implicate CTLA-4 engagement in the regulation of T cell adhesion to APCs and endothelial cells (25, 26). However, one study on tolerized T cells in a diabetes model found no effect of anti–CTLA-4 on breaking tolerance or helper T cell–APC interactions in vivo, although the timing of the intervention may be responsible for the lack of effect (27). The effects of anti–CTLA-4 on T cell dynamics in the setting of effective immunotherapy are unknown.

Ionizing radiation (IR) therapy is a standard treatment modality for many cancers. A number of mechanisms have been proposed for the effects of IR, including stimulation of antitumor immunity (28–30). Antigen-specific mechanisms include promoting

Conflict of interest: The authors have declared that no conflict of interest exists.
Citation for this article: *J Clin Invest.* 2012;122(10):3718–3730. doi:10.1172/JCI61931.

the presentation of tumor-derived antigens through immunogenic tumor cell death and alteration of antigen presentation in surviving tumor cells (29, 31–33). Non-antigen-specific mechanisms include contributing to the effector phase of the antitumor immune response by enhancing the expression of relevant soluble and cell surface ligands. For example, chemokines, adhesion molecules, and co-stimulatory ligands are all upregulated by IR (31, 32, 34–38). However, there are no data on the effects of IR on TIL interactions with tumor cells in vivo.

We have utilized a previously established 4T1 breast carcinoma mouse model in which IR synergizes with anti–CTLA-4 mAb treatment (10, 39) to visualize the impact of anti–CTLA-4 immunotherapy under conditions where it fails as a monotherapy or succeeds as a combination therapy with IR. *Cxcr6*$^{+/gfp}$ knock-in BALB/c mice were used as recipients to allow tracking of relevant TILs (34). We show that anti–CTLA-4 mAb as monotherapy increased T cell motility in vivo, whereas the combination of IR and anti–CTLA-4 mAb promoted synergistic T cell arrest in contact with tumor cells. TIL arrest and reduction of 4T1 tumor growth were blocked by anti-NKG2D antibodies. These results are consistent with clinical observations that unhindered NKG2D recognition is important for the success of anti–CTLA-4 therapy (40) and suggest that a combination of cell-intrinsic TCR-CD8, CTLA-4, and NKG2D signals synergize to regulate TIL recognition of tumor cells.

Results

Visualizing endogenous TILs in a mouse model of antitumor therapy. 4T1 tumors and their metastases are inhibited by antitumor CD8$^+$ T cells in mice treated with local IR and anti–CTLA-4 mAb in combination, but not as single modalities (10). We have previously shown that the majority of CD8$^+$ T cells present in the tumors that are being rejected are CXCR6$^+$ (34). Therefore, we employed mice with the CXCR6 coding sequence replaced by GFP (41) at one allele and WT *Cxcr6* at the other allele (*Cxcr6*$^{+/gfp}$) to visualize TILs by intravital TPLSM with minimal interference to homing (34, 42). To visualize tumor cells, we prepared 4T1 cells expressing cyan fluorescent protein (CFP), which can be readily distinguished from GFP by TPLSM (43). CFP-4T1 tumors growing in *Cxcr6*$^{+/gfp}$ mice were rejected with a kinetics similar to that of the parental 4T1 tumors growing in WT mice (10, 34) upon treatment with local IR and anti–CTLA-4 mAb 9H10 (IR+9H10), with the immune-mediated regression phase becoming apparent after day 20 (Figure 1, A and B). Ex vivo characterization of CD8$^+$ TILs on day 21 showed that the GFP$^+$ subset was highly enriched for cells expressing the activation marker CD69 in both untreated and local IR+9H10-treated mice (Figure 1C). Importantly, GFP$^+$CD69$^+$ cells represented a larger portion of CD8$^+$ TILs and were increased greater than 4-fold in the tumors of treated mice (Figure 1D). In addition, ex vivo measurement of IFN-γ production by intracellular staining without additional stimulation showed that IFN-γ–positive CD8$^+$ cells are present almost exclusively within the GFP$^+$CD69$^+$ subset (Figure 1E), suggesting that this subset contains antigen-specific antitumor T cells (4).

To analyze the dynamic behavior of T cells in the tumor microenvironment, we first imaged tumors on day 22 after implantation. CFP$^+$ 4T1 cells were readily detectable in mice that were untreated or treated with local IR only or 9H10 only (Figure 1F and Supplemental Videos 1 and 2; supplemental material available online with this article; doi:10.1172/JCI61931DS1). In marked contrast, treatment with the combination of local IR+9H10 induced a dramatic reduction in CFP$^+$ 4T1 cells, consistent with the observed tumor regression (Figure 1F and Supplemental Videos 1 and 2). We restricted our analysis of GFP$^+$ TIL behavior to a qualitative description, since we were not able to make meaningful comparisons in the absence of tumor cells in the combination treatment. The GFP$^+$ TILs in the untreated, irradiated, and 9H10-treated tumors behaved similarly, with rapid movement in the connective tissue and a mixed pattern of intermediate movement and arrest in the tumor (Supplemental Videos 1 and 2). Consistent with previous data indicating that anti–CTLA-4 mAb in combination with vaccination, but not as monotherapy, results in increased intratumoral T cell infiltration (44), only the combination of IR and 9H10 resulted in a significant increase ($P < 0.005$, IR+9H10 versus control) in GFP$^+$ cells (Figure 1G), and these were highly motile throughout the connective tissue space (Supplemental Videos 1 and 2). There were few opportunities to observe these cells interacting with tumor cells. Imaging on day 22 indicated that failure to control the tumor in untreated and single modality–treated tumors was not due to loss of TILs displaying a range of interaction modes with tumor cells. In addition, observation of tumor sites that were successfully treated by the combination of IR and 9H10 demonstrates persistence of highly active immune effector cells that continue to survey the tumor-free connective tissue.

Effect of radiotherapy and anti–CTLA-4 treatment on the interactions of TILs with tumor cells. Since most 4T1 cells had disappeared from tumors treated with IR+9H10 on day 22, at least from the outermost portion of the tumor that can be imaged, TPLSM was next performed on day 16, after administration of local IR and the first dose of 9H10 (Figure 1A). During imaging, we defined the tumor parenchyma based on the CFP signal and included some surrounding connective tissue, which often contained postcapillary venules with rolling leukocytes, in each video. We defined TILs stringently as GFP$^+$ cells within areas containing CFP$^+$ cells, recorded their behavior over a period of 15 minutes, and performed a comprehensive analysis of T cell migratory properties under different treatment conditions. The 15-minute period was adequate to assess motility of TILs versus arrest (<1.5 μm/min) in the tumor and allowed sampling of 4 fields in each tumor preparation.

On day 16, the number and composition of GFP$^+$ cells were similar in all of the conditions examined, with the majority of GFP$^+$ T cells being CD8$^+$ cells expressing the activation markers CD69 and/or NKG2D (Supplemental Figure 1, A–C). GFP$^+$ cells moved randomly with higher speed in vascularized connective tissue than within the CFP$^+$ tumor cell–rich areas in all conditions (Supplemental Videos 3 and 4, and Supplemental Figure 1B). All analyses were performed on cells present within the tumor as defined by the presence of CFP$^+$ tumor cells. Analysis of the migratory paths showed that GFP$^+$ TILs moved longer distances in mice treated with local IR only or 9H10 only than in untreated mice (Figure 2A). Unexpectedly, the increase in migratory activity elicited by each monotherapy was reversed when local IR and 9H10 were used in combination. Consistent with this, compared with the untreated controls (average speed, 2.61 ± 1.88 μm/min), GFP$^+$ TILs of irradiated tumors displayed significantly increased motility (average speed, 3.62 ± 2.19 μm/min, $P = 0.001$) and slightly decreased arrest coefficient (36% in control to 31% in IR-treated, $P = 0.5$). This effect was accounted for by the increased motility of GFP$^+$ TILs in less vascularized tumor regions. The increase in motility of GFP$^+$ TILs was even more prominent in mice treated with 9H10 alone (average speed, 6.95 ± 2.94 μm/min, $P < 0.0001$ versus control), which

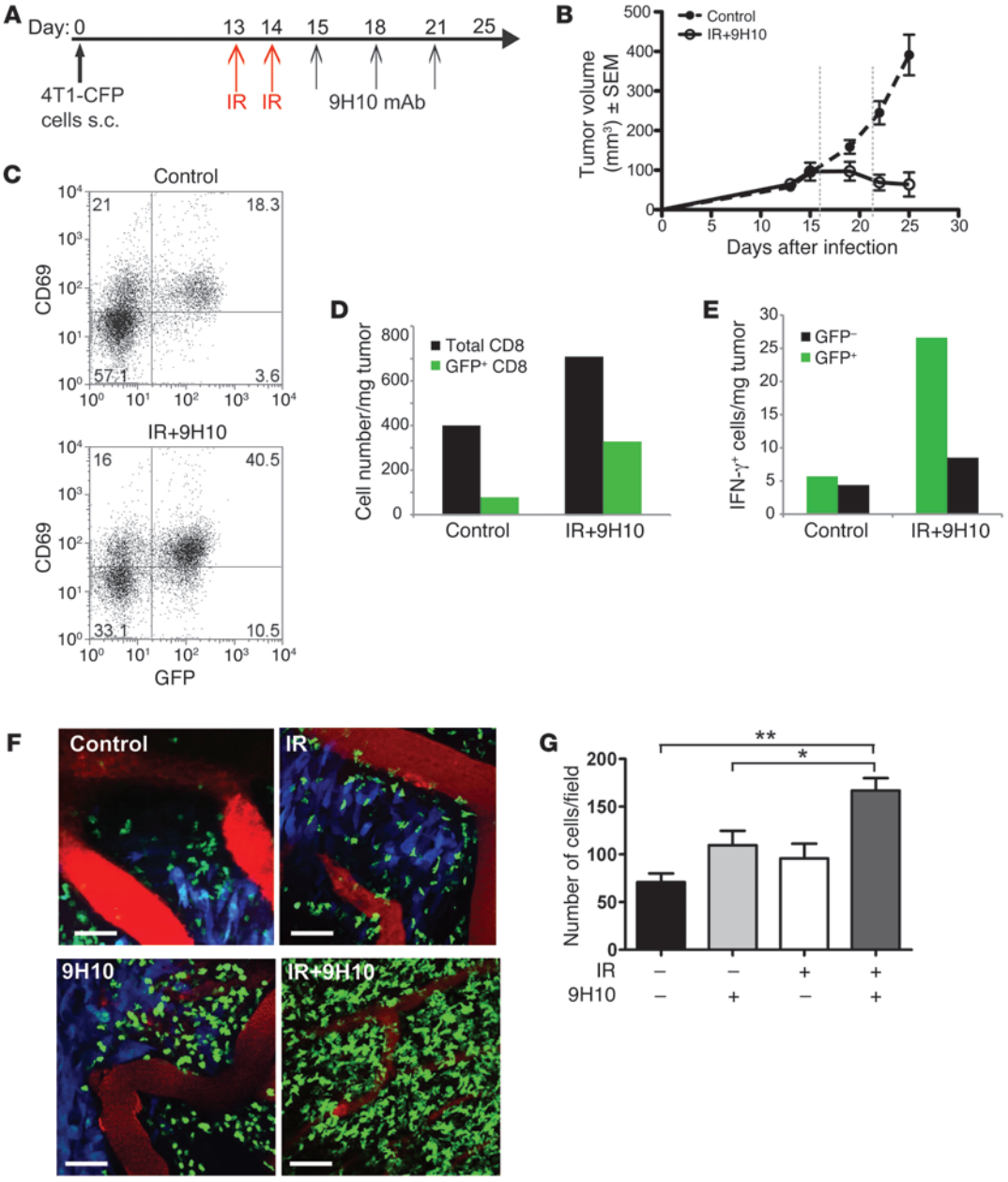

Figure 1

Characterization of 4T1-CFP tumor model for imaging CD8⁺ TILs in *Cxcr6*$^{+/gfp}$ mice treated with local radiotherapy and anti–CTLA-4 mAb. (**A**) Treatment schedule. (**B**) Growth of 4T1-CFP tumors of untreated and IR+9H10-treated mice (n = 6/group). Treated mice showed significant tumor inhibition (P = 0.0006). Vertical dashed lines indicate the days at which in vivo TPLSM was performed. (**C**–**E**) Ex vivo characterization of CD8 TILs on day 21. Samples were gated on CD8⁺ T cells. (**C**) Most GFP⁺ TILs express CD69, and represent a greater proportion of CD8⁺ cells in tumors treated with IR+9H10 than controls. (**D**) IR+9H10 treatment increases the density of CD8⁺ TILs about 1.8-fold, but the density of CD8 GFP⁺ TILs is increased by more than 4-fold. (**E**) The majority CD8⁺ TILs producing IFN-γ are GFP⁺, as determined by intracellular staining. Error bars are absent because pooling of tumors within each group was necessary to obtain sufficient number of cells for analysis. Results are from 10 mice/group and are representative of 2 experiments. (**F**) In vivo TPLSM images of GFP⁺ TILs in 4T1-CFP tumors on day 22 (Supplemental Videos 1 and 2). Mice were mock treated (Control) or treated as indicated. Images are representative of 6–8 independent experiments for each treatment. Scale bars: 58 μm. T cells are green (GFP), 4T1 cells are blue (CFP), blood vessels are red (quantum dots). (**G**) Quantification of GFP⁺ TILs on day 22. Results are the mean ± SD of 9 fields (9 × 10⁴ μm²) from 3 mice per group. *P < 0.05, **P < 0.005.

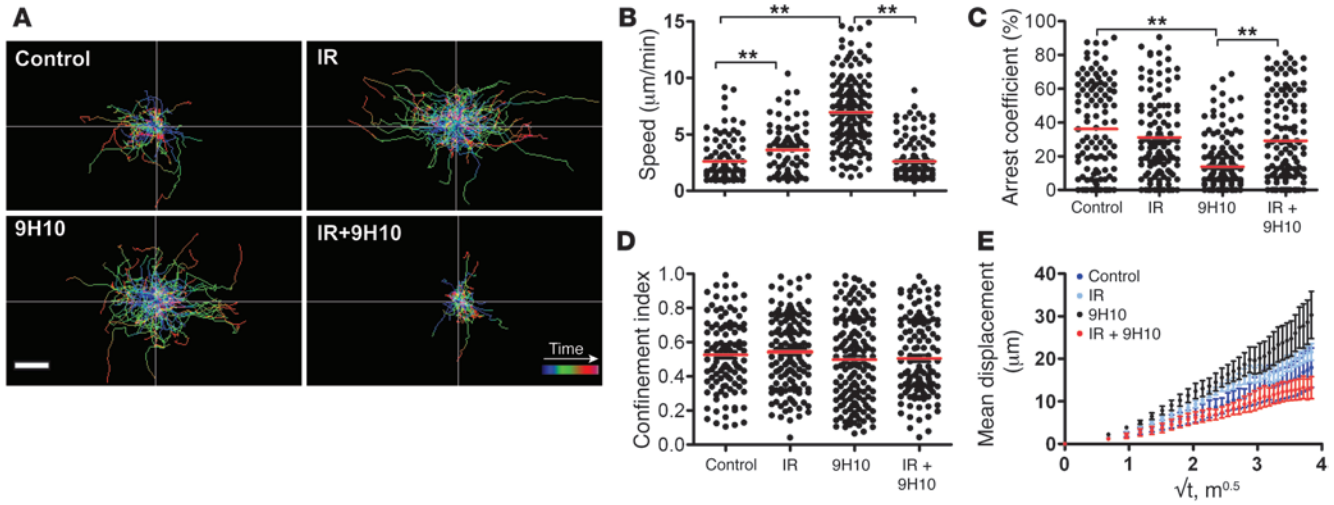

Figure 2

Treatment with IR and 9H10 alters the migratory behavior of TILs. *Cxcr6*$^{+/gfp}$ mice injected with 4T1-CFP cells and treated as described in Figure 1A were imaged on day 16. Movement of individual cells was tracked in the *xy* plane through stacks of 3D time-lapse images. Data are derived from 4 mice for each treatment. Each time lapse lasted 15 minutes and was acquired as a *z*-stack of 30 μm between 60 and 90 μm of depth below the capsule. (**A**) Trajectories of individual GFP$^+$ TILs in CFP$^+$ cell–rich areas (Supplemental Videos 3 and 4). The color scale shows time length of each path. Both IR and 9H10 as single treatment led to increased path lengths compared with controls. In contrast, when given in combination, IR+9H10 led to reduced migration of GFP$^+$ TILs. Scale bar: 30 μm. Scatter plots of mean velocity (**B**), arrest coefficient (**C**), and confinement index (**D**) of GFP$^+$ TILs in tumor cell–rich areas. The arrest coefficient was defined as the percentage of time a cell was moving at a speed less than 1.5 μm/min. Each data point represents a single cell, and red bars indicate mean values. **P* < 0.05, ***P* < 0.005. (**E**) Random walk analysis. Mean displacement plotted as a function of the square root of time. The slope of each line represents the motility coefficient *M* and indicates the area an average cell scans per unit time. A liner curve indicates a random walk, a plateau indicates confinement, and a higher slope indicates directed motion.

also showed a significant decrease in arrest coefficient (36% in controls versus 13% in 9H10-treated, $P < 0.0001$) (Figure 2, B and C, and Supplemental Videos 3 and 4). However, when 9H10 was given to mice that had also received local IR, the increased motility seen with 9H10 alone was abrogated (average speed, 2.59 ± 1.74 μm/min in double-treated mice, $P < 0.0001$ versus 9H10 alone), and the arrest coefficient significantly increased (from 13% with 9H10 alone to 29% in double-treated mice, $P < 0.0001$). There was no significant difference in speed and arrest coefficient between control and IR+9H10-treated mice. The confinement index was not significantly altered in any of the treatment groups, and mean displacement was consistent with a random walk (Figure 2, D and E).

In vivo imaging demonstrated that 9H10 used as monotherapy delivered a "go" signal to GFP$^+$ TILs, which was converted to a significant "stop" signal (defined as cells moving at ≤1.5 μm/min) in irradiated tumors, despite the fact that IR alone also increased GFP$^+$ TIL motility. Many of the TILs in IR+9H10-treated mice appeared fully arrested for the 15-minute duration of the imaging sessions (Supplemental Videos 3 and 4). Importantly, all arrested TILs displayed active protrusions consistent with an active arrest process, such as formation of a cytotoxic synapse (45), rather than loss of viability, as was previously reported for non-antigen-specific T cells in tumors (2). These data suggest that treatment with 9H10 disrupts the stable, long-lasting interactions between T cells and tumor cells that are required for antitumor effector functions (2, 4, 5), but these interactions are restored by radiation-induced changes.

T cell arrest in contact with tumor cells is MHC-I dependent. In vivo imaging on day 16 demonstrated that GFP$^+$ TILs form stable interactions with tumor cells in untreated mice as well as in mice treated with IR+9H10, but only the latter are able to inhibit tumor growth. To test whether T cell arrest requires MHC recognition, we injected mice with a cocktail of function-blocking antibodies to all expressed MHC-I alleles (H-2K^d, H-2D^d, H-2L^d) or an isotype control 18 hours before imaging. These antibodies are targeted to the α3 domain and thus block the critical contribution of CD8 to peptide-MHC–dependent killing and cytokine production (46, 47). Treatment with MHC-I blocking mAbs markedly lengthened the migratory paths of GFP$^+$ TILs in both untreated mice and in mice treated with IR+9H10 (Figure 3A). GFP$^+$ TIL motility in control mice was significantly increased in the presence of anti–MHC-I mAbs compared with isotype mAbs (5.27 ± 2.12 versus 2.06 ± 1.11 μm/min, $P < 0.0001$), and the arrest coefficient dropped from 50% to 11% ($P < 0.0001$) (Figure 3, B and C). Likewise, GFP$^+$ TIL motility in IR+9H10-treated mice was significantly increased in the presence of anti–MHC-I mAbs compared with isotype mAbs (4.82 ± 1.39 versus 2.5 ± 1.13 μm/min, $P < 0.0001$), and the arrest coefficient dropped from 35% to 12% ($P < 0.0001$). There was no significant difference in average GFP$^+$ TIL speed and arrest coefficient between control and IR+9H10-treated mice that had received anti–MHC-I mAbs. These results suggest that arrest of GFP$^+$ TILs requires the interaction of CD8 with MHC-I molecules on tumor cells. Availability of MHC-I does not seem to depend on IR, as TILs in untreated control and treated mice showed similar behavior.

Radiotherapy upregulates ICAM-1 and induces RAE-1 on 4T1 tumor cells in vivo. To identify molecular candidates that could account for the observed synergy of radiotherapy with anti–CTLA-4 mAb in increasing the stability of TIL interaction with tumor cells, we analyzed IR-induced changes in the expression of surface molecules known to participate in recognition of target cells by CD8$^+$

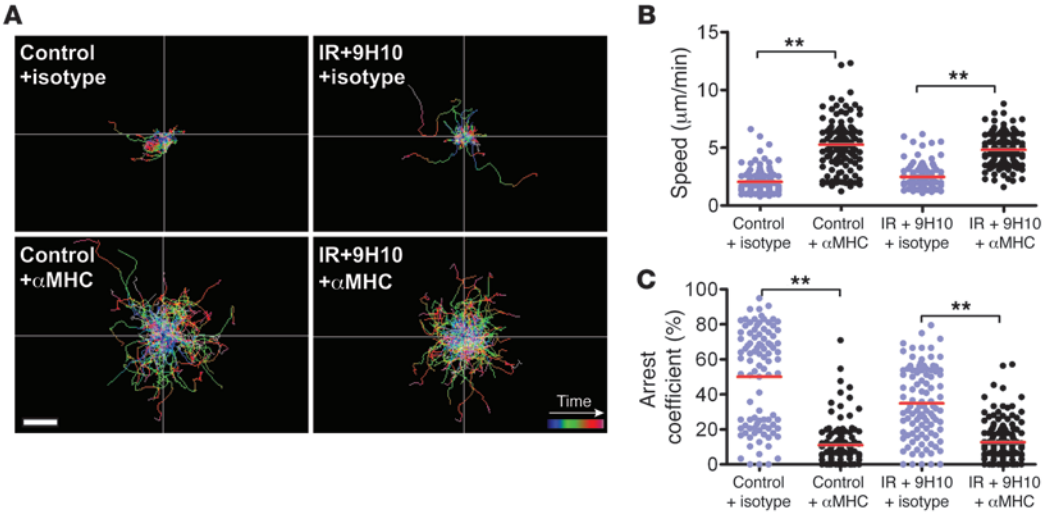

Figure 3

T cell arrest requires MHC-I recognition. *Cxcr6*$^{+/gfp}$ mice injected with 4T1-CFP cells and treated as described in Figure 1A were imaged on day 16. Migratory behavior of GFP$^+$ TILs was analyzed 18 hours after injection of MHC-I blocking mAbs or irrelevant isotype mAb in untreated control mice and mice treated with IR+9H10, as indicated. Data were derived from 4 mice for each treatment. (**A**) Trajectories of individual GFP$^+$ TILs, and scatter plots of mean velocity (**B**) and arrest coefficient (**C**). MHC blockade resulted in increased T cell migration in both treated and untreated mice. Each data point represents a single cell, and red bars indicate mean values. $^{**}P < 0.005$.

effectors on 4T1 cells. Radiation has been shown to upregulate the expression of MHC-I and ICAM-1 (32, 33, 35, 36). In addition, genotoxic stress, such as induced by IR, regulates the expression of NKG2D ligands on normal and transformed cells (37, 38). Therefore, these molecules were chosen for analysis.

CFP$^+$ 4T1 cells were isolated from tumors 48 hours after IR on day 16 and analyzed by flow cytometry with gating on CFP$^+$ and CD45$^-$ cells (Figure 4A). 4T1 cells growing in vivo showed significant phenotypic changes compared with in vitro cultured cells, with increased expression of H2-K^d and ICAM-1, but loss of the NKG2D ligands retinoic acid early inducible–1 (RAE-1) and H60 (Figure 4B), whereas MULT-1 was not expressed in vitro or in vivo (Supplemental Figure 2 and data not shown). Levels of H2-K^d were not further increased after in vivo irradiation, whereas basal ICAM-1 expression on 4T1 cells from non-irradiated tumors was significantly increased on 4T1 cells from irradiated tumors (Figure 4A). RAE-1 was effectively absent or barely detectable on 4T1 cells from non-irradiated tumors and was increased significantly on 4T1 cells from irradiated tumors (Figure 4A). In contrast, radiation did not induce the expression of H60, which was not detectable in vivo despite expression of H60 in cultured cells (Figure 4B). The low level of RAE-1 is typical of the expression pattern for this stress-induced ligand (37, 48, 49). In support of the possibility that RAE-1 might contribute to tumor recognition, approximately 60% of GFP$^+$ CD8$^+$ T cells expressed NKG2D in the tumor (Supplemental Figure 1). Expression of NKG2D on activated TILs did not depend upon treatment with 9H10 or IR, since it was similar in TILs in all treatment groups.

RAE-1 enhances TCR stop signal in the presence of anti–CTLA-4 mAb in vitro. Our in vivo data indicated that anti–CTLA-4 mAb enhances GFP$^+$ TIL motility and reduces their contact time with tumor cells, but this effect is reversed by prior tumor irradiation (Figure 2 and Supplemental Videos 3 and 4). To determine whether the interaction between radiation-induced RAE-1 and NKG2D plays a role in regulating CD8$^+$ T cell motility, we performed a well-established in vitro motility assay that allows monitoring the movements of preactivated CD8$^+$ T cells migrating on a planar surface coated with ICAM-1 (24, 50). The average speed of T cells (9.05 ± 5.74 μm/min) was significantly reduced by the addition of anti-CD3 mAb (average speed, 2.29 ± 1.40 μm/min, $P < 0.0001$) (Figure 5, A and B), consistent with the known ability of TCR to deliver a stop signal (50). In contrast, 9H10 alone significantly increased T cell motility (average speed, 11.96 ± 6.35 μm/min, $P < 0.0001$). Importantly, 9H10 was able to override the TCR-induced stop signal when given together with anti-CD3 (average speed, 8.62 ± 3.98 μm/min, $P < 0.0001$ versus anti-CD3) (Figure 5, A and B), as previously described (24). We then tested the effects of RAE-1 on T cell motility in this assay. The addition of RAE-1 did not alter the motility of T cells migrating on ICAM-1 without additional treatment (average speed, 8.08 ± 4.40 μm/min, $P = 0.57$) or treated with 9H10 (average speed 11.85 ± 6.46 μm/min, $P = 0.74$ versus 9H10) (Figure 5, A and B). However, the addition of RAE-1 significantly decreased the motility of cells treated with 9H10 and anti-CD3 mAbs (average speed, 3.64 ± 2.47 μm/min, $P < 0.0001$ versus anti-CD3+9H10) (Figure 5B). This effect was specific for RAE-1, because the addition of the chemokine CXCL16 did not significantly change the speed of T cells migration over ICAM-1 in the presence of 9H10 and anti-CD3 mAbs (11.22 ± 5.69 versus 11.26 ± 5.23 μm/min, $P = 0.63$) (Supplemental Figure 3). These results suggest that NKG2D engagement can promote T cell arrest under conditions where anti–CTLA-4–mediated go signals are dominant over TCR-mediated stop signals.

NKG2D is required for the synergy of radiotherapy and anti–CTLA-4 mAb treatment in vivo. We next tested whether NKG2D ligation can provide the radiation-induced signal that counteracts 9H10-induced motility leading to TIL arrest in 4T1 tumors in vivo. To this end, the anti-NKG2D mAb CX5 was injected into mice shortly before intravital imaging on day 16. CX5 treatment did not affect the motility of GFP$^+$ TILs in untreated control mice (Figure 5C and Supplemental Videos 5 and 6). In contrast, CX5 treatment

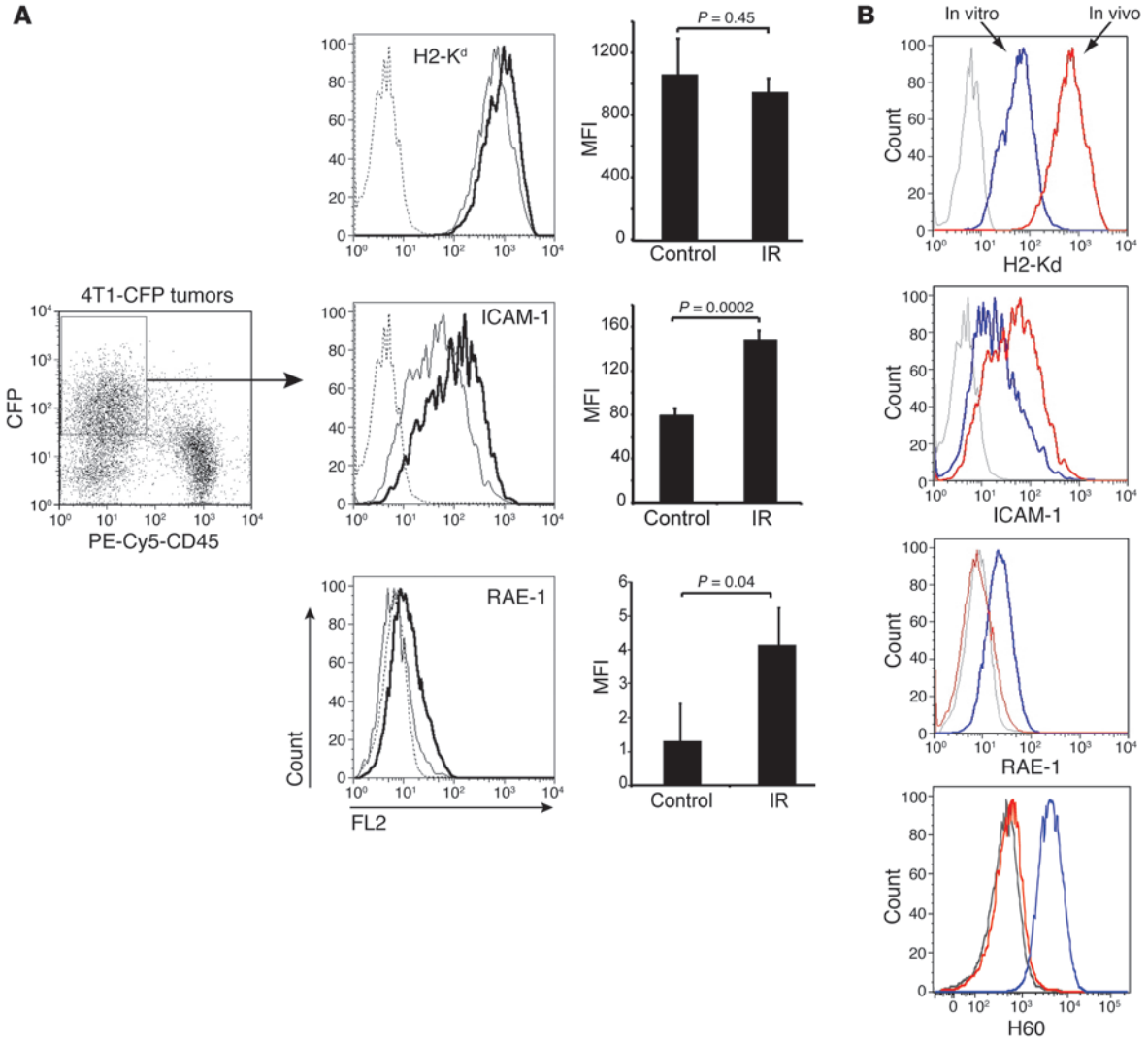

Figure 4

Upregulation of ICAM-1 and RAE-1γ on 4T1 cells after in vivo irradiation. *Cxcr6*$^{+/gfp}$ mice were injected s.c. with CFP$^+$ 4T1 cells on day 0 and mock treated (Control) (n = 9) or treated with local IR in 2 doses of 12 Gy on days 13 and 14 (n = 9). Tumors were analyzed on day 16. To obtain sufficient material, we pooled tumors from 3 mice in each treatment group to obtain 3 independent samples. Data are representative of 3 experiments. (**A**) 4T1 tumor cells were identified as CFP$^+$CD45$^-$. Histograms show the expression of H2-K^d, ICAM-1, and RAE-1γ on the gated CFP$^+$CD45$^-$ mock-treated (thin lines) and irradiated (bold lines) cells. Cells stained with isotype control (dashed lines). Bar graphs show MFI after subtraction of background of 3 samples ± SD. In vivo irradiation significantly increased ICAM-1 but not H2-K^d and induced the expression of RAE-1γ on 4T1 cells. (**B**) Expression of H2-K^d, ICAM-1, RAE-1γ, and H60 was compared in CFP$^+$ 4T1 tumor cells cultured in vitro (blue lines) and CFP$^+$ 4T1 tumor cells isolated from tumors implanted in mice (red lines). Gray lines, isotype control. H60 and RAE-1 molecules were equally undetectable on 4T1 cells from in vivo growing tumors digested with liberase or dissociated with EDTA, as described in Methods. Data are representative of 3 experiments.

prevented T cells from stopping and arresting with tumor cells in mice treated with IR+9H10. Compared with mice that did not receive CX5 (Figure 2, A–C), blocking the NKG2D receptor in mice treated with IR+9H10 (Figure 5D) significantly increased the average speed of GFP$^+$ TILs (2.59 ± 1.74 to 4.89 ± 2.96 μm/min, $P < 0.0001$) and decreased the arrest coefficient (29% to 18%, $P < 0.0001$). Therefore, blocking the NKG2D receptor on T cells significantly reversed the ability of IR to promote a stable interaction of T cells with tumor cells after CTLA-4 ligation. This suggests that RAE-1 induction is a critical step whereby IR synergizes with anti–CTLA-4 treatment.

NKG2D blockade abrogates tumor inhibition induced by IR+9H10 treatment. To determine whether NKG2D-dependent interactions of TILs with tumor cells were required for the therapeutic effect of IR+9H10 treatment, NKG2D receptor was blocked by administration of CX5 starting on day 15 after tumor inoculation. In the absence of treatment with 9H10, CX5 did not have any significant effect on growth of the primary s.c. tumor or spontaneous lung metastases by itself ($P > 0.05$, CX5 versus control) or in combination with IR ($P > 0.05$, CX5+IR versus IR) (Figure 6, A–C). However, administration of CX5 to mice treated with IR+9H10 significantly reversed the immune-mediated inhibition of the primary

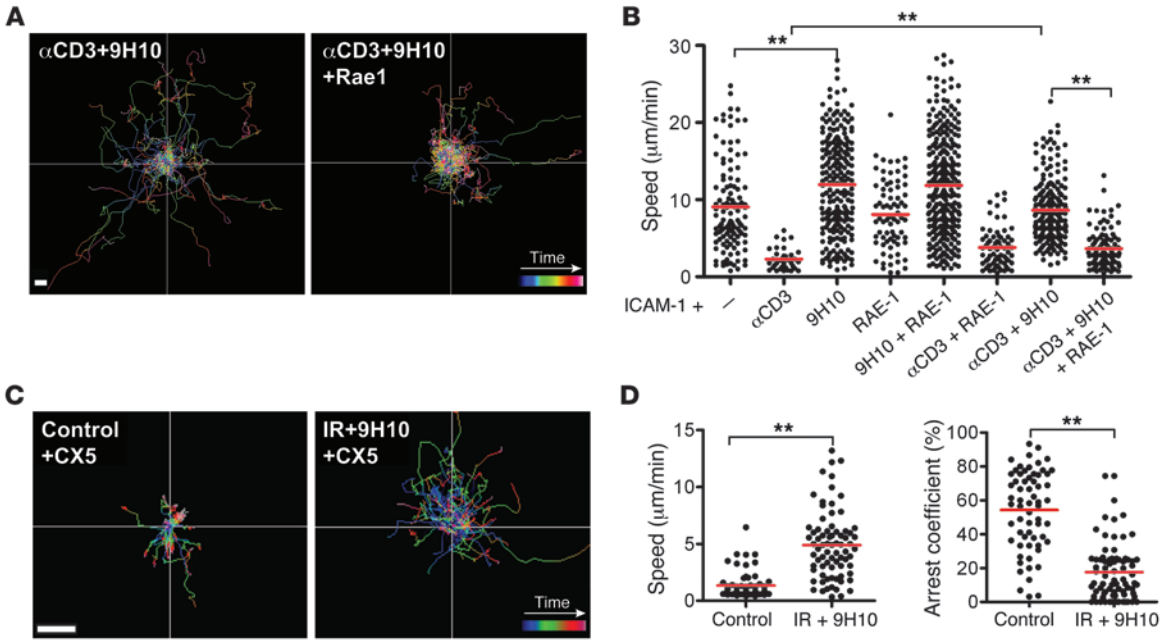

Figure 5

RAE-1/NKG2D interactions promote T cell arrest in the presence of TCR ligation and 9H10. (**A** and **B**) In vitro analysis of T cell motility. Migration of preactivated CD8$^+$ T cells over an ICAM-1–coated glass surface. Trajectories (**A**) and mean velocity (**B**) of individual CD8$^+$ T cells stimulated with anti-CD3 and/or 9H10 in the absence or presence of RAE-1β, as indicated. Paths were tracked over time from confocal 2D time lapses. Each line corresponds to the path of an individual cell. Each dot represents the average speed of a cell tracked over 15 minutes. Data are representative of 3 independent experiments. Scale bar: 10 μm. (**C** and **D**) In vivo analysis of T cell motility. *Cxcr6*$^{+/gfp}$ mice were injected with 4T1-CFP cells on day 0 and left untreated or treated with IR+9H10 as described in Figure 2, and tumors were imaged by TPLSM on day 16 (Supplemental Videos 5 and 6). All mice received an i.p. injection of NKG2D blocking mAb CX5 30 minutes before imaging. (**C**) Trajectories of individual GFP$^+$ TILs show that CX5 treatment led to increased migratory activity in mice treated with IR+9H10 but not in control mice. Scale bar: 30 μm. (**D**) Scatter plots showed increased speed and decreased arrest coefficient of TILs in the presence of NKG2D blockade in tumors of mice treated with IR+9H10. Data are derived from analysis of 3 mice per treatment group. Each data point represents a single cell, and red bars indicate mean values. $^{**}P < 0.005$.

irradiated tumor ($P < 0.0005$, IR+9H10 versus IR+9H10+CX5), and tumors grew in these mice similarly to tumors of mice that had received local IR without 9H10 ($P = 0.1643$) (Figure 6A). Interestingly, blockade of NKG2D also significantly reduced metastasis inhibition in mice treated with IR+9H10 ($P < 0.05$, IR+9H10+CX5 versus IR+9H10), though a trend to have an effect was still present ($P = 0.0624$, IR+9H10+CX5 versus control), suggesting that CD8-mediated control of lung metastases (10) is at least partially dependent on NKG2D (Figure 6, B and C).

Overall, our results identify the interaction between radiation-induced RAE-1 on tumor cells and NKG2D on TILs as a key molecular mechanism that explains the ability of radiotherapy to promote immune-mediated inhibition of tumor growth and metastasis in mice treated with anti–CTLA-4 mAbs.

Discussion

Here we employed the poorly immunogenic 4T1 carcinoma as a model to define novel mechanisms that account for the therapeutic effects of treatment with anti–CTLA-4 mAb by studying the behavior of TILs in mice treated with 9H10 alone (tumor growth) versus 9H10+IR (inhibition of tumor growth). The results of this experiment could not be predicted based on earlier in vitro and in vivo studies with CTLA-4–expressing cells or anti–CTLA-4 (7, 10, 13–20, 24). The results suggest a new axis for control of antitumor reactivity in CD8$^+$ T cells based on combinatorial control by CTLA-4 and NKG2D ligands in tumors. Anti–CTLA-4 resulted in significant acceleration of TIL motility within the tumor. Local IR also weakly enhanced motility. In contrast, IR synergized with anti–CTLA-4 mAb to arrest TILs in tumors in vivo. MHC-I and NKG2D-mediated recognition were also required for this arrest. We propose that TILs activated by anti–CTLA-4 require TCR-CD8 and NKG2D signals for recognition within the tumor leading to arrest. Data from in vitro motility assays (Figure 5, A and B) further support this hypothesis.

Other investigators have utilized TPLSM to examine the dynamics of antigen-specific T cells within tumors expressing model antigens or viral antigens to which strong antigen-specific T cell responses are generated. Mrass et al. found that antigen-specific T cells were capable of both migrating through tumors and forming stable interactions of more than 30 minutes with tumor cells prior to induction of killing (2). OT-1 T cells required 6 hours to kill EL-4 lymphoma cells expressing ovalbumin in vivo (4, 5). Stable immunological synapses are 3-fold more efficient than more dynamic CTL-target interactions in vitro (51). Thus, the destabilization of TIL-4T1 cell interactions that we have observed with anti–CTLA-4 mAb could increase the time required to kill a tumor cell to 18 hours, tipping the balance in favor of tumor growth. Our results indicating that stable interactions induced by IR+9H10

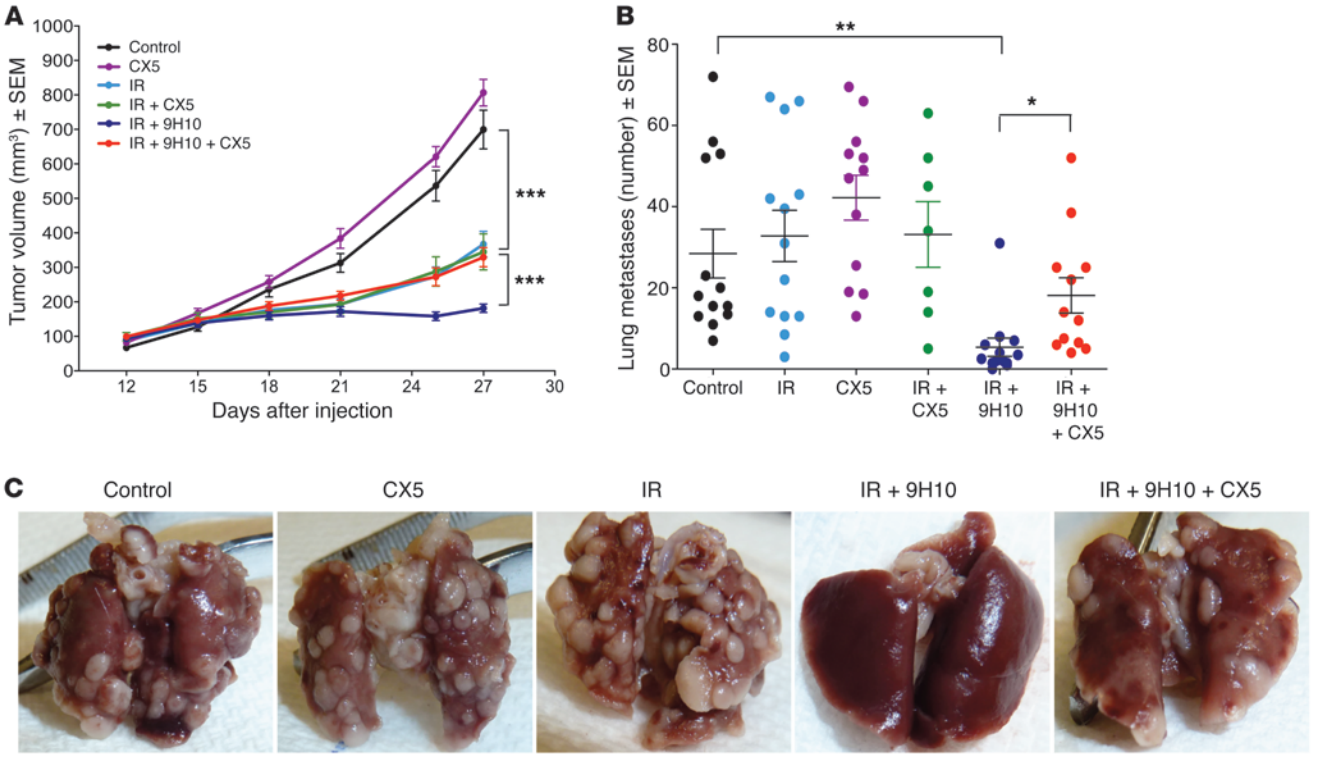

Figure 6

Blocking NKG2D abrogates immune-mediated inhibition of the irradiated primary tumor in mice treated with IR+9H10 and reduces metastasis inhibition. WT mice inoculated with parental 4T1 cells on day 0 (n = 7–13/group) were randomly assigned to different treatments, as indicated. IR was delivered in 2 fractions of 12 Gy to the s.c. tumors on day 12 and 13. Anti–CTLA-4 mAb 9H10 was given i.p. on days 15, 18, and 21. Anti-NKG2D mAb CX5 was given i.p. on days 15, 18, 21, 25, and 28. (**A**) Tumor volume is shown as the mean ± SEM at each time within each treatment group. CX5 by itself did not have any effect on tumor growth ($P > 0.05$, CX5 versus control). IR by itself caused significant tumor growth inhibition ($P < 0.0005$, IR versus control) that was not altered by CX5 ($P = 0.4349$, CX5+IR versus IR) but was significantly enhanced in the presence of 9H10 ($P < 0.0005$, IR+9H10 versus IR). The latter effect was completely abrogated by addition of CX5 ($P = 0.1643$, IR+9H10+CX5 versus IR). (**B**) The number of surface lung metastases was not significantly altered by IR or CX5 used alone ($P > 0.05$ versus control) or by IR in combination with CX5 ($P > 0.05$ versus control). IR+9H10 caused a significant inhibition of lung metastases ($P < 0.005$, IR+9H10 versus all other groups) that was partially abrogated by addition of CX5 ($P < 0.05$, IR+9H10 versus IR+9H10+CX5). Data shown are from 2 independent experiments combined. Bars indicate the mean ± SEM. *$P < 0.05$, **$P < 0.005$, ***$P < 0.0005$. (**C**) Images of lungs from representative animals in each treatment group, as indicated.

correlated with tumor inhibition are consistent with these calculations. We also observed TIL arrest in the absence of contact with tumor cells, suggesting that TILs may also target stromal elements to undermine the tumor, a process promoted by radiation-induced cross-presentation of tumor antigens by stromal cells (52).

The 4T1 cell line is a variant of a mammary tumor that arose spontaneously in BALB/c mice and has no known viral or foreign antigens (53). This is the first study to our knowledge of the interaction of TILs with a syngeneic tumor expressing an endogenous antigen repertoire. While tracking of endogenous TILs has some drawbacks, in that antigen recognition may not be a constant, this approach is necessary to gain insights as to why anti–CTLA-4 therapy fails or succeeds in the context of a response to a non-immunogenic tumor. We have previously shown that in *Cxcr6*$^{+/gfp}$ mice the majority of GFP$^+$ TILs that infiltrate 4T1 tumors are CD8$^+$ T cells, and that CD8$^+$ but not CD4$^+$ T cells are required for tumor rejection (10, 34). Importantly, on day 16 GFP$^+$ TILs present at the periphery of the tumor monitored by imaging were predominantly CD8$^+$ (Supplemental Figure 1C). While both tumor-specific and nonspecific CD8$^+$ T cells can infiltrate tumors, only tumor-specific CD8$^+$ T cells express CD69 (4). The fact that CD69 was expressed by almost all GFP$^+$ TILs (Figure 1C) indicates that this subset of TILs is highly enriched in antigen-specific CD8$^+$ T cells in both untreated and IR+9H10-treated mice. In support of this notion, blocking CD8 recognition of MHC-I increased motility of most GFP$^+$ TILs, suggesting that coordinated TCR-CD8 recognition of MHC-I regulates the dynamic behavior of T cells in this model (Figure 3). We have previously shown that in vivo mAb-mediated blockade of the α3 domain of MHC-I selectively increases the speed of antigen-specific CD8$^+$ T cells, but not bystander T cells (54). While it is conceivable that CD8 interactions with MHC-I could contribute to CD8$^+$ T cell arrest independent of antigen recognition by TCR, thus far CD8-mediated adhesion in T cells has always been tightly linked to antigen recognition (55). The presence of activated TILs in the untreated 4T1 tumors, which are generally considered non-immunogenic, may seem surprising. However, the presence of tumor-specific CD8$^+$ T cells that are unable to prevent tumor growth in the absence of intervention is well known in human cancers (56), including breast cancer (57).

Notably, GFP$^+$ T cells present in the tumors of untreated mice on day 16 were not different in terms of numbers or expression of CD69 and NKG2D from GFP$^+$ TILs of IR+9H10-treated mice (Supplemental Figure 1, A and B). Therefore, it is likely that at this early time anti–CTLA-4 mAb was acting on effector-memory CD8$^+$ T cells that were spontaneously primed during tumor growth (58). Although GFP$^+$ TILs of both untreated and IR+9H10-treated mice were able to establish stable, MHC-I–dependent contacts with 4T1 cells (Figure 3), only in IR+9H10-treated tumors were the interactions between GFP$^+$ TILs and tumor cells dependent on NKG2D (Figure 5, C and D). Increased TIL motility seen in mice treated with IR alone might be due to alterations in the molecular and physical signals in the tumor microenvironment. For instance, increased oxygenation in the tumor after radiation (59) could influence T cell motility (60). Importantly, in mice treated with IR alone, GFP$^+$ TILs did not form stable interactions with tumor cells, despite the increased expression of RAE-1γ on the latter, suggesting that CTLA-4 co-engagement with NKG2D is a requirement for arrest in IR- or IR+9H10-treated mice.

The molecular mechanism of these effects requires further study. Interestingly, recent data suggest that interaction of CTLA-4 with the natural ligands CD80 and/or CD86 may either hinder or promote T cell motility, depending on the cellular context. In one study, interaction of CTLA-4 with CD86 expressed on endothelial cells promoted T cell adhesion to endothelial cells (25). In another, CTLA-4 interaction with CD80 and CD86 expressed by APCs impaired stable contacts of T cells with APCs (26). Since 4T1 cells do not express CD80 or CD86 (Supplemental Figure 2), the effect of anti–CTLA-4 mAb on the interaction of TILs with tumor cells cannot be explained by inhibition of the interaction of CTLA-4 or CD28 with these costimulatory molecules. In vitro, the addition of soluble anti–CTLA-4 mAb increased the motility of purified preactivated CD8$^+$ T cells migrating over ICAM-1–coated surface and reversed the stop signal of anti-CD3 ligation (Figure 5B), suggesting that the mAb can deliver a "go" signal by binding to CTLA-4 as previously shown (24). Based on these data, Rudd proposed that the therapeutic antitumor effects of anti–CTLA-4 mAb might be due, in part, to reduced dwell time between CTLs and their targets, allowing for faster turnaround time of tumor cell killing (61). Our in vivo data do not support this hypothesis, since reduced TIL motility was associated with IR+9H10-mediated reduction in tumor growth, while increased TIL motility in mice treated with 9H10 alone was not (10). Instead, our data provide evidence for a context-dependent regulation of T cell motility by CTLA-4, which is modulated by co-ligation of NKG2D. Integrin activation may be one component of this effect (21, 62).

RAE-1 is a member of a family of NKG2D ligands that are usually absent from normal cells but expressed on transformed, infected, or distressed cells (48) and are thought to play a pivotal role in helping the host discriminate "self" from "abnormal self" by stimulating NK cell lysis and/or providing a co-stimulatory signal to CD8$^+$ T cells (48). Importantly, NKG2D has been shown to play a key role in the formation of an immunological synapse between effector and target cells in conditions of suboptimal ligation by either ICAM-1 or antigen (63, 64), suggesting that its engagement may complement weak signals from target cells. In addition, the ectopic expression of RAE-1 and other NKG2D ligands was shown to induce the rejection of several progressively growing, transplantable tumors, highlighting a critical role of the NKG2D receptor-ligand system in antitumor immunity (65). Interestingly, Deguine et al. (66) recently reported that rejection of EL4 lymphoma cells ectopically expressing RAE-1 is mediated by NK cells and requires very short interactions between NK cells and their targets, highlighting the different requirements for killing by CTLs and NK cells. We have previously shown that the rejection of 4T1 tumors in mice treated with IR+9H10 requires CD8$^+$ T cells (10). The elevated levels of MHC-I present on 4T1 cells in vivo may protect these tumor cells from NK cell lysis (Figure 4). Interestingly, the tumor microenvironment in vivo influences the phenotype of 4T1 cells, leading to an increase in MHC-I and ICAM-1 and loss of RAE-1 and H60 expression as compared with in vitro cultured cells (Figure 4). Immunosuppressive inflammatory-type monocytes (CD11b$^+$IL-4Ra$^+$), which are present within 4T1 tumors and produce IL-13 and IFN-γ, may be responsible for some of these changes (67). Consistent with this possibility, IFN-γ has been reported to downregulate H60 on tumors, and H60 downregulation was required together with increased MHC-I expression to enhance tumor cell resistance to NK-mediated killing (68).

Successful control of the primary tumor in mice treated with IR+9H10 also reduced the non-irradiated metastases of 4T1 (Figure 6 and ref. 10). Reduction of metastases may arise from increased priming of naive tumor-specific T cells by the in situ vaccination generated by IR (29, 31), as well as the improvement of tumor-specific CD8$^+$ memory T cells by anti–CTLA-4 (20). In fact, the increased tumor infiltration by activated CD8$^+$ T cells seen on day 21 (Figure 1) in mice treated with IR+9H10 is consistent with the pro-proliferative effects of anti–CTLA-4 when used in combination with vaccination (69). Interestingly, NKG2D blockade did not significantly alter the number of lung metastases by itself but reduced the inhibition of lung metastases in mice treated with IR+9H10 (Figure 6, B and C). Several contributing factors may explain this. An effect of the immune response on seeding of metastatic cells from the primary tumor cannot be ruled out. However, in our experience, surgical resection of 4T1 tumors on day 14 after implantation does not significantly reduce lung metastases, consistent with a prior report (70). Alternatively, it is possible that the increased early killing by existing TILs that is dependent on NKG2D in mice treated with IR+9H10 is important for eventually increasing the level of antitumor T cells required to inhibit metastases (71). In addition, the marked inhibition of the primary tumor obtained with IR+9H10 may relieve the TGF-β–mediated suppression of RAE-1 expression (72), leading to upregulated expression of RAE-1 on lung metastases. This explanation is consistent with the NKG2D-mediated lung metastasis rejection by IL-21–activated NK cells seen after surgical resection of the primary 4T1 tumor (73).

Our data provide insights about the factors that regulate the effectiveness of anti–CTLA-4 treatment. We have defined the dominance of the "go" signal as a potential mechanism of failure for tumors that do not express NKG2D ligands and/or strong antigens, while the success of anti–CTLA-4 monotherapy may reflect the tumor expression of higher-affinity antigens and/or basal levels of NKG2D ligands. Importantly, our data provide a mechanism for the synergy of anti–CTLA-4 with strategies to enhance NKG2D ligand expression on tumor cells. The relevance of this approach is highlighted by emerging clinical experience indicating that the NKG2D receptor-ligand system plays an important role in the response of melanoma patients treated with anti–CTLA-4 (40). On the other hand, experimental data showing that RAE-1 expression in pancreatic islets is critical for development of autoimmune diabetes (49) suggest that normal tissue expression of

NKG2D ligands may also determine the pattern of autoimmune toxicity associated with anti–CTLA-4 mAb treatment in cancer patients. In support of this possibility, the intestinal epithelium shows constitutive expression of NKG2D ligands (74), and colitis is a common immune-related adverse event in patients treated with the anti–CTLA-4 mAb ipilimumab (75). Improved understanding of the crosstalk between CTLA-4 and NKG2D will help in the development of strategies to enhance the therapeutic index of anti–CTLA-4 treatments.

Methods

Tumor implantation and treatment. Six- to 8-week-old BALB/c mice were purchased from Taconic. *Cxcr6*$^{+/gfp}$ mice (41) in the BALB/c background were bred in house. Mice were injected s.c. in the right flank with 5×10^4 4T1 cells (10) or 10^5 CFP$^+$ 4T1 (4T1-CFP) cells generated by retroviral gene transfer in 0.1 ml DMEM without additives on day 0. Perpendicular tumor diameters were measured with a Vernier caliper, and tumor volumes were calculated as length × width^2 × 0.52. Local radiotherapy was delivered in 2 doses of 12 Gy each on days 13 and 14, as previously described (10, 34) with some modifications (76). Briefly, all mice (including controls) were lightly anesthetized by i.p. injection of Avertin (240 mg/kg) and positioned on a dedicated Plexiglas tray. Radiotherapy was delivered to a field including the tumor with 5-mm margins using a Clinac 2300 C/D Linear Accelerator (Varian Medical Systems) fitted with a 25-mm RadioSurgery conical collimator (BrainLAB AG), which is designed to deliver very sharp and limited radiation dose fields. Superflab bolus (1.5 cm tissue equivalent material) was placed over the tumor, and a source-to-skin distance (SSD) of 100 cm was set. Radiation was delivered at 600 cGy/min with 6-MV X-rays. Anti–CTLA-4 mAb 9H10 (77) was given i.p. at 200 μg, as indicated. The blocking anti-mouse NKG2D CX5 mAb (49) (BioLegend) was given i.p. at 200 μg, as indicated. Lungs were harvested at the end of the experiment, determined as the day when at least 1 mouse in any of the groups appeared moribund due to excessive metastatic burden. Two investigators used a dissecting microscope to independently count lungs surface metastatic nodules after formalin fixation, as described previously (10).

For imaging, *Cxcr6*$^{+/gfp}$ mice were injected with 4T1-CFP cells s.c. about 0.5 cm dorsal to the inguinal lymph node and treated with IR and/or 9H10 as described above. Mice imaged on day 16 received 1 dose of 9H10 on day 15, whereas mice imaged on day 22 received 2 doses (day 15 and 18). In some experiments, CX5 mAb was injected i.p. at 200 μg shortly before imaging. Anti–MHC-I α3 domain (LEAF purified anti-H2-L^d clone 28-14-8, anti-H2-K^d clone SF1-1.1, and anti-H2-D^d clone 34-2-12; BioLegend) or isotype control mAbs were injected i.p. each at 500 μg/mouse (total, 1,500 μg/mouse), approximately 18 hours before imaging.

Surgery. The surgical procedure to expose the implanted tumor was similar to the procedure previously utilized for imaging of the inguinal lymph node (43, 78). Briefly, mice were anesthetized with 100 mg ketamine, 15 mg xylazine, and 2.5 mg acepromazine per kilogram body weight and restrained on a stage warmer at 37°C (BioTherm Micro S37, Biogenics). The abdominal skin was incised from the edge of the rib cage through the midline to the thigh. A skin flap was separated from the abdominal muscle to expose the tumor. To stabilize, moisturize, and maintain the tumor at 37°C, we placed the skin flap on a thermoconductive base made of silicone elastomer (Sylgard 184, Dow Corning) surrounding a core of thermoconductive putty (T-putty 502, Thermagon). A saline-filled chamber consisting of a coverslip glued to a nylon washer was mounted on the skin flap over the tumor. 100% oxygen was provided to mice by mask to compensate for anesthesia-induced respiratory depression.

Intravital microscopy. Tumors were imaged with a Bio-Rad Radiance multiphoton microscope fitted with a Tsunami pulsed laser (Spectraphysics) and controlled by LaserSharp 2000 software (Bio-Rad) and a Nikon 40× objective (water immersed; numerical aperture, 0.8). For imaging of GFP and CFP, the excitation wavelength was set to 910 nm. Polyethylene glycol–coated quantum dots (Qtracker 655, Quantum Dot) were injected for visualization of blood flow. To create time-lapse sequences, we typically scanned volumes of tissue 30 × 400 × 400 μm at 5-μm *z*-steps and 30-second intervals.

In vitro migration assays. CD8$^+$ T cells specific for *Listeria monocytogenes* p60 antigen (79) were purified from L9.6 TCR transgenic mice on a BALB/c *Rag*$^{-/-}$ background using MACS untouched CD8$^+$ T cell cocktail (Miltenyi Biotec). 10^6 purified T cells were stimulated using 2.5×10^7 irradiated splenocytes, 25 U/ml IL-2, and 10 nM p60 peptide 217–225. T cells were used on day 4 after stimulation. All peptide-stimulated T cells expressed NKG2D. Cover glasses were coated with 10 μM full-length ICAM-1 for 1 hour at room temperature, washed with PBS, and then blocked with 25% human serum albumin for 30 minutes at room temperature (80). The cover glass was then mounted on a FCS2 flow chamber (Bioptechs), and cells were washed and resuspended in binding buffer (1× HBSS + 10 mM HEPES + 1 mM $CaCl_2$ + 1 mM $MgCl_2$+ 0.2% BSA) containing the mAb for imaging. Images were acquired with a confocal laser system (LSM 510, Zeiss). In vitro motility analyses on ICAM-1–coated surfaces were done as previously described (50). The cells were left untreated or treated with anti-CD3 (40 μg/ml), anti–CTLA-4 (50 μg/ml), or both during the time of imaging (15 minutes). In some experiments 10 μg/ml recombinant mouse RAE-1β (R&D system) or recombinant mouse CXCL16 (PeproTech) was spotted on the glass and left overnight at 4°C prior to coating with ICAM-1 and use in the motility assays. The affinity of RAE-1β and RAE-1γ for NKG2D is similar (81).

Data analysis. Cell movement was analyzed with Volocity (Improvision) and Imaris (Bitplane) software for the in vivo and the in vitro data, respectively. For calculation of cell speed, the coordinates of each cell were determined in two dimensions based on maximum pixel projections and tracked over time, and motility parameters were calculated. Average cell velocity was calculated as described previously (82). Individual cells were considered independent experiments. Cells were characterized as immobile if their average velocity was less than 1.5 μm/min. The arrest coefficient was calculated as the percentage of each track in which the cell moved more slowly than 1.5 μm/min (83). The confinement index was calculated as the ratio of maximum displacement to path length (83). The mean displacement, plotted against the square root of the time, and the motility coefficient were calculated as described (84).

Flow cytometry. Tumors were minced into small pieces and digested with 0.2 mg/ml DNase and 1.67 Wünsch U/ml Liberase (Roche) as previously described (34, 85). Obtained cell suspensions were filtered through a 40-μm nylon cell strainer and red blood cells lysed. Fixable Viability Dye eFluor 660 (catalog 65-0864, eBioscience) was used to distinguish live and dead cells. For analysis of 4T1-CFP cells, aliquots of 10^6 cells from in vivo growing tumors or in vitro culture were incubated with anti-mouse CD16/32 (Fc block) for 10 minutes, followed by staining with various antibodies at 4°C for 30 minutes. PE-conjugated CX1 anti-mouse RAE-1γ or isotype control (eBioscience), PE-conjugated anti-mouse H60 or isotype control (R&D Systems), PE–ICAM-1, PE–H2-K^d (BD Biosciences — Pharmingen), MULT-1–PE, CD80-APC or CD86–Alexa Fluor 488 (all from eBioscience) were used. FITC– or PE–Cy5-CD45 (BD Biosciences — Pharmingen) was used to separate infiltrating stromal cells from the cancer cells. In some experiments, to exclude the possibility that the loss of H60 and RAE-1 on 4T1 cells in vivo was due to sensitivity to the enzymes used for tumor digestion, tumors were dissociated using a cocktail of 5 mM EDTA supplemented with the metalloproteinase inhibitor BB94 (Batimastat) (20 μM) and edelfosine/ET-18-OCH_3, a selective inhibitor for phosphatidylinositol-phospholipase C (10 μM final concentration) for 15 minutes at 37°C in

a shaker. For analysis of MULT-1, CD80, and CD86 expression, in vitro cultured 4T1 cells were treated with 1 dose of 12-Gy IR and harvested and analyzed 24 hours later.

For analysis of CD8 TILs, $CD8^+$ T cells were purified from 4T1-CFP tumor–derived cell suspensions using CD8α (Ly-2) MicroBeads (Miltenyi Biotec), following the manufacturer's protocol. Obtained cells were incubated for 2 hours in the presence of 1 μl/ml of brefeldin A, washed and incubated with rat anti-mouse CD16/CD32 mAb (2.4G2) to block nonspecific binding, and then stained with CD8α–PE-Cy5 and CD69-PE, followed by intracellular staining with IFN-γ–PE-Cy7 or isotype control antibodies according to the manufacturer's instructions (BD Biosciences — Pharmingen). The density of CD8 GFP^+ and GFP^- T cells in the tumors was calculated by dividing the total number of obtained cells by the tumor weight.

In some experiments, after tumor digestion, cell suspensions were enriched for lymphocytes by CD45 MicroBeads (Miltenyi Biotec) and stained with CD3–Alexa Fluor 700, CD8-APC, CD69–PE-Cy7, CD4–PE-Cy7, NKG2D-PE, or isotype control antibodies (eBioscience). For flow analysis of NKG2D expression, samples were gated on GFP^+CD8^+ cells. All samples were analyzed using a LSR II flow cytometer and FlowJo version 6.4.7 or 8.8.3 (Tree Star).

Statistics. In vivo and in vitro tracking data were analyzed using nonparametric tests; the Kruskal-Wallis nonparametric test was used for overall multiple group comparisons, followed by the Mann-Whitney test for 2-group comparisons. A linear mixed effects model for repeated-measures data (86) using the mouse as the analytic unit was employed to confirm the results.

Random coefficients regression (RCR) was used to model log tumor volume as a function of elapsed time from treatment onset and to compare treatments with respect to tumor growth rate. Log volume was used as the dependent variable, since its change was well approximated as linear. The RCR model included elapsed time as a numeric factor, treatment as a classification factor, and the interaction of treatment with time. The interaction term was partitioned to compare treatments in terms of tumor growth rate. The correlation structure imparted by repeated measurement was modeled by assuming observations to be correlated only when acquired from the same animal, with the strength of correlation inversely dependent on the elapsed time between observations. Analysis of covariance (ANCOVA) was used to compare treatment arms in terms of the assessment of lung metastases on day of euthanasia. A Shapiro-Wilk test was used to verify the assumption that the residuals from each ANCOVA follow a Gaussian distribution. All reported *P* values are 2 sided and were declared statistically significant at the 5% level. The statistical computations were carried out using R 2.9.1 (http://www.r-project.org/) and SAS, version 9.0 (SAS Institute) software.

Study approval. The Institutional Animal Care and Use Committee of New York University approved all experiments involving mice.

Acknowledgments

We thank Kaushik Choudhuri for providing helpful suggestions and E. Pamer for the L9.6 mice. We thank P. Lopez and the staff of the NYU Cancer Institute Flow Cytometry facility for their expert assistance. We thank K. DeWyngaert and the personnel the Department of Radiation Oncology at NYU Langone Medical Center and School of Medicine (New York, New York, USA) for their expert assistance. This work was supported by NIH grants R01CA113851 (to S. Demaria), R01AI55037 (to M.L. Dustin), PN2EY016586 (to M.L. Dustin), and 5 P30CA16087 (Flow Cytometry and Microscopy Cores); Research Scholar Award RSG-05-145-01-LIB from the American Cancer Society (to S. Demaria); a grant from the Chemotherapy Foundation (to S. Demaria); postdoctoral fellowships from Boehringer Ingelheim (to M.G. Ruocco); and Department of Defense Breast Cancer Research Program Fellowship W81XWH-10-1-0007 (to K.A. Pilones).

Received for publication November 14, 2011, and accepted in revised form July 12, 2012.

Address correspondence to: Sandra Demaria, Department of Pathology, MSB-521, NYU School of Medicine, 550 First Avenue, New York, New York 10016, USA. Phone: 212.263.7308; Fax: 212.263.8211; E-mail: Sandra.Demaria@nyumc.org. Or to: Michael L. Dustin, Skirball Institute for Biomolecular Medicine, 540 First Avenue, New York, New York 10016, USA. Phone: 212.263.3207; Fax: 212.263.5711; E-mail: Michael.Dustin@nyumc.org.

Maria Grazia Ruocco's present address is: Université Pierre et Marie Curie, CNRS UMR7211, and INSERM U959, Bat. CERVI, Hôpital Pitié-Salpêtrière, Paris, France.

Julie Huang's present address is: University Medical Center Utrecht, Heidelberglaan, Utrecht, The Netherlands.

1. Galon J, et al. Type, density, and location of immune cells within human colorectal tumors predict clinical outcome. *Science*. 2006;313(5795):1960–1964.
2. Mrass P, et al. Random migration precedes stable target cell interactions of tumor-infiltrating T cells. *J Exp Med*. 2006;203(12):2749–2761.
3. Ng LG, Mrass P, Kinjyo I, Reiner SL, Weninger W. Two-photon imaging of effector T-cell behavior: lessons from a tumor model. *Immunol Rev*. 2008;221:147–162.
4. Boissonnas A, Fetler L, Zeelenberg IS, Hugues S, Amigorena S. In vivo imaging of cytotoxic T cell infiltration and elimination of a solid tumor. *J Exp Med*. 2007;204(2):345–356.
5. Breart B, Lemaître F, Celli S, Bousso P. Two-photon imaging of intratumoral CD8+ T cell cytotoxic activity during adoptive T cell therapy in mice. *J Clin Invest*. 2008;118(4):1390–1397.
6. FDA approves new treatment for a type of late-stage skin cancer [press release]. U.S. Food and Drug Administration Web Site. http://www.fda.gov/NewsEvents/Newsroom/PressAnnouncements/ucm1193237.htm. Published March 25, 2011. Accessed July 27, 2012.
7. Peggs KS, Quezada SA, Allison JP. Cell intrinsic mechanisms of T-cell inhibition and application to cancer therapy. *Immunol Rev*. 2008;224:141–165.
8. van Elsas A, Hurwitz AA, Allison JP. Combination immunotherapy of B16 melanoma using anti-cytotoxic T lymphocyte-associated antigen 4 (CTLA-4) and granulocyte/macrophage colony-stimulating factor (GM-CSF)-producing vaccines induces rejection of subcutaneous and metastatic tumors accompanied by autoimmune depigmentation. *J Exp Med*. 1999;190(3):355–366.
9. Mokyr MB, Kalinichenko T, Gorelik L, Bluestone JA. Realization of the therapeutic potential of CTLA-4 blockade in low-dose chemotherapy-treated tumor-bearing mice. *Cancer Res*. 1998;58(23):5301–5304.
10. Demaria S, et al. Immune-mediated inhibition of metastases after treatment with local radiation and CTLA-4 blockade in a mouse model of breast cancer. *Clin Cancer Res*. 2005;11(2 pt 1):728–734.
11. Wing K, et al. CTLA-4 control over Foxp3+ regulatory T cell function. *Science*. 2008;322(5899):271–275.
12. Qureshi OS, et al. Trans-endocytosis of CD80 and CD86: a molecular basis for the cell-extrinsic function of CTLA-4. *Science*. 2011;332(6029):600–603.
13. Chambers CA, Kuhns MS, Egen JG, Allison JP. CTLA-4-mediated inhibition in regulation of T cell responses: mechanisms and manipulation in tumor immunotherapy. *Annu Rev Immunol*. 2001;19:565–594.
14. Egen JG, Allison JP. Cytotoxic T lymphocyte antigen-4 accumulation in the immunological synapse is regulated by TCR signal strength. *Immunity*. 2002;16(1):23–35.
15. Pentcheva-Hoang T, Egen JG, Wojnoonski K, Allison JP. B7-1 and B7-2 selectively recruit CTLA-4 and CD28 to the immunological synapse. *Immunity*. 2004;21(3):401–413.
16. Teft WA, Kirchhof MG, Madrenas J. A molecular perspective of CTLA-4 function. *Annu Rev Immunol*. 2006;24:65–97.
17. Martin M, Schneider H, Azouz A, Rudd CE. Cytotoxic T lymphocyte antigen 4 and CD28 modulate cell surface raft expression in their regulation of T cell function. *J Exp Med*. 2001;194(11):1675–1681.
18. Chikuma S, Imboden JB, Bluestone JA. Negative regulation of T cell receptor-lipid raft interaction by cytotoxic T lymphocyte-associated antigen 4. *J Exp Med*. 2003;197(1):129–135.
19. Hegel JK, Knieke K, Kolar P, Reiner SL, Brunner-Weinzierl MC. CD152 (CTLA-4) regulates effector functions of CD8+ T lymphocytes by repressing Eomesodermin. *Eur J Immunol*. 2009;39(3):883–893.

20. Pedicord VA, Montalvo W, Leiner IM, Allison JP. Single dose of anti-CTLA-4 enhances CD8+ T-cell memory formation, function, and maintenance. *Proc Natl Acad Sci U S A*. 2011;108(1):266–271.
21. Schneider H, Valk E, da Rocha Dias S, Wei B, Rudd CE. CTLA-4 up-regulation of lymphocyte function-associated antigen 1 adhesion and clustering as an alternate basis for coreceptor function. *Proc Natl Acad Sci U S A*. 2005;102(36):12861–12866.
22. Wei B, da Rocha Dias S, Wang H, Rudd CE. CTL-associated antigen-4 ligation induces rapid T cell polarization that depends on phosphatidylinositol 3-kinase, Vav-1, Cdc42, and myosin light chain kinase. *J Immunol*. 2007;179(1):400–408.
23. Schneider H, Valk E, Leung R, Rudd CE. CTLA-4 activation of phosphatidylinositol 3-kinase (PI 3-K) and protein kinase B (PKB/AKT) sustains T-cell anergy without cell death. *PLoS One*. 2008; 3(12):e3842.
24. Schneider H, et al. Reversal of the TCR stop signal by CTLA-4. *Science*. 2006;313(5795):1972–1975.
25. Lozanoska-Ochser B, Klein NJ, Huang GC, Alvarez RA, Peakman M. Expression of CD86 on human islet endothelial cells facilitates T cell adhesion and migration. *J Immunol*. 2008;181(9):6109–6116.
26. Poirier N, et al. Inducing CTLA-4-dependent immune regulation by selective CD28 blockade promotes regulatory T cells in organ transplantation. *Sci Transl Med*. 2010;2(17):17ra10.
27. Fife BT, et al. Interactions between PD-1 and PD-L1 promote tolerance by blocking the TCR-induced stop signal. *Nat Immunol*. 2009;10(11):1185–1192.
28. Demaria S, Bhardwaj N, McBride WH, Formenti SC. Combining radiotherapy and immunotherapy: a revived partnership. *Int J Radiat Oncol Biol Phys*. 2005;63(3):655–666.
29. Apetoh L, et al. Toll-like receptor 4-dependent contribution of the immune system to anticancer chemotherapy and radiotherapy. *Nat Med*. 2007; 13(9):1050–1059.
30. Formenti SC, Demaria S. Systemic effects of local radiotherapy. *Lancet Oncol*. 2009;10(7):718–726.
31. Lugade AA, Moran JP, Gerber SA, Rose RC, Frelinger JG, Lord EM. Local radiation therapy of B16 melanoma tumors increases the generation of tumor antigen-specific effector cells that traffic to the tumor. *J Immunol*. 2005;174(12):7516–7523.
32. Reits EA, et al. Radiation modulates the peptide repertoire, enhances MHC class I expression, and induces successful antitumor immunotherapy. *J Exp Med*. 2006;203(5):1259–1271.
33. Garnett CT, Palena C, Chakraborty M, Tsang KY, Schlom J, Hodge JW. Sublethal irradiation of human tumor cells modulates phenotype resulting in enhanced killing by cytotoxic T lymphocytes. *Cancer Res*. 2004;64(21):7985–7994.
34. Matsumura S, et al. Radiation-induced CXCL16 release by breast cancer cells attracts effector T cells. *J Immunol*. 2008;181(5):3099–3107.
35. Hareyama M, et al. Effect of radiation on the expression of carcinoembryonic antigen of human gastric adenocarcinoma cells. *Cancer*. 1991;67(9):2269–2274.
36. Gaugler MH, Squiban C, van der Meeren A, Bertho JM, Vandamme M, Mouthon MA. Late and persistent up-regulation of intercellular adhesion molecule-1 (ICAM-1) expression by ionizing radiation in human endothelial cells in vitro. *Int J Radiat Biol*. 1997;72(2):201–209.
37. Gasser S, Orsulic S, Brown EJ, Raulet DH. The DNA damage pathway regulates innate immune system ligands of the NKG2D receptor. *Nature*. 2005;436(7054):1186–1190.
38. Kim JY, et al. Increase of NKG2D ligands and sensitivity to NK cell-mediated cytotoxicity of tumor cells by heat shock and ionizing radiation. *Exp Mol Med*. 2006;38(5):474–484.
39. Pilones KA, Kawashima N, Yang AM, Babb JS, Formenti SC, Demaria S. Invariant natural killer T cells regulate breast cancer response to radiation and CTLA-4 blockade. *Clin Cancer Res*. 2009; 15(2):597–606.
40. Jinushi M, Hodi FS, Dranoff G. Therapy-induced antibodies to MHC class I chain-related protein A antagonize immune suppression and stimulate antitumor cytotoxicity. *Proc Natl Acad Sci U S A*. 2006; 103(24):9190–9195.
41. Unutmaz D, Xiang W, Sunshine MJ, Campbell J, Butcher E, Littman DR. The primate lentiviral receptor Bonzo/STRL33 is coordinately regulated with CCR5 and its expression pattern is conserved between human and mouse. *J Immunol*. 2000; 165(6):3284–3292.
42. Geissmann F, et al. Intravascular immune surveillance by CXCR6+ NKT cells patrolling liver sinusoids. *PLoS Biol*. 2005;3(4):e113.
43. Shakhar G, et al. Stable T cell-dendritic cell interactions precede the development of both tolerance and immunity in vivo. *Nat Immunol*. 2005;6(7):707–714.
44. Quezada SA, Peggs KS, Curran MA, Allison JP. CTLA4 blockade and GM-CSF combination immunotherapy alters the intratumor balance of effector and regulatory T cells. *J Clin Invest*. 2006; 116(7):1935–1945.
45. Stinchcombe JC, Bossi G, Booth S, Griffiths GM. The immunological synapse of CTL contains a secretory domain and membrane bridges. *Immunity*. 2001; 15(5):751–761.
46. Bilsborough J, Van Pel A, Uyttenhove C, Boon T, Van den Eynde BJ. Identification of a second major tumor-specific antigen recognized by CTLs on mouse mastocytoma P815. *J Immunol*. 1999; 162(6):3534–3540.
47. Ozato K, Evans GA, Shykind B, Margulies DH, Seidman JG. Hybrid H-2 histocompatibility gene products assign domains recognized by alloreactive T cells. *Proc Natl Acad Sci U S A*. 1983;80(7):2040–2043.
48. Diefenbach A, Jamieson AM, Liu SD, Shastri N, Raulet DH. Ligands for the murine NKG2D receptor: expression by tumor cells and activation of NK cells and macrophages. *Nat Immunol*. 2000;1(2):119–126.
49. Ogasawara K, et al. NKG2D blockade prevents autoimmune diabetes in NOD mice. *Immunity*. 2004; 20(6):757–767.
50. Dustin ML, Bromley SK, Kan Z, Peterson DA, Unanue ER. Antigen receptor engagement delivers a stop signal to migrating T lymphocytes. *Proc Natl Acad Sci U S A*. 1997;94(8):3909–3913.
51. Beal AM, et al. Protein kinase C theta regulates stability of the peripheral adhesion ring junction and contributes to the sensitivity of target cell lysis by CTL. *J Immunol*. 2008;181(7):4815–4824.
52. Zhang B, et al. Induced sensitization of tumor stroma leads to eradication of established cancer by T cells. *J Exp Med*. 2007;204(1):49–55.
53. Aslakson CJ, Miller FR. Selective events in the metastatic process defined by analysis of the sequential dissemination of subpopulations of a mouse mammary tumor. *Cancer Res*. 1992;52(6):1399–1405.
54. Kim JV, Kang SS, Dustin ML, McGavern DB. Myelomonocytic cell recruitment causes fatal CNS vascular injury during acute viral meningitis. *Nature*. 2009;457(7226):191–195.
55. Yachi PP, Ampudia J, Gascoigne NR, Zal T. Nonstimulatory peptides contribute to antigen-induced CD8-T cell receptor interaction at the immunological synapse. *Nat Immunol*. 2005;6(8):785–792.
56. Rosenberg SA, et al. Use of tumor-infiltrating lymphocytes and interleukin-2 in the immunotherapy of patients with metastatic melanoma. A preliminary report. *N Engl J Med*. 1988;319(25):1676–1680.
57. Mahmoud SM, et al. Tumor-infiltrating CD8+ lymphocytes predict clinical outcome in breast cancer. *J Clin Oncol*. 2011;29(15):1949–1955.
58. Chambers CA, Sullivan TJ, Truong T, Allison JP. Secondary but not primary T cell responses are enhanced in CTLA-4-deficient CD8+ T cells. *Eur J Immunol*. 1998;28(10):3137–3143.
59. Withers HR. The four R's of radiotherapy. *Adv Radiat Biol*. 1975;5(3):241–271.
60. Huang JH, et al. Requirements for T lymphocyte migration in explanted lymph nodes. *J Immunol*. 2007;178(12):7747–7755.
61. Rudd CE. The reverse stop-signal model for CTLA4 function. *Nat Rev Immunol*. 2008;8(2):153–160.
62. Dillon TJ, Carey KD, Wetzel SA, Parker DC, Stork PJ. Regulation of the small GTPase Rap1 and extracellular signal-regulated kinases by the costimulatory molecule CTLA-4. *Mol Cell Biol*. 2005; 25(10):4117–4128.
63. Somersalo K, et al. Cytotoxic T lymphocytes form an antigen-independent ring junction. *J Clin Invest*. 2004;113(1):49–57.
64. Markiewicz MA, et al. Costimulation through NKG2D enhances murine CD8+ CTL function: similarities and differences between NKG2D and CD28 costimulation. *J Immunol*. 2005;175(5):2825–2833.
65. Diefenbach A, Jensen ER, Jamieson AM, Raulet DH. Rae1 and H60 ligands of the NKG2D receptor stimulate tumour immunity. *Nature*. 2001; 413(6852):165–171.
66. Deguine J, Breart B, Lemaître F, Di Santo JP, Bousso P. Intravital imaging reveals distinct dynamics for natural killer and CD8(+) T cells during tumor regression. *Immunity*. 2010;33(4):632–644.
67. Gallina G, et al. Tumors induce a subset of inflammatory monocytes with immunosuppressive activity on CD8+ T cells. *J Clin Invest*. 2006;116(10):2777–2790.
68. Bui JD, Carayannopoulos LN, Lanier LL, Yokoyama WM, Schreiber RD. IFN-dependent down-regulation of the NKG2D ligand H60 on tumors. *J Immunol*. 2006;176(2):905–913.
69. Peggs KS, Quezada SA, Korman AJ, Allison JP. Principles and use of anti-CTLA4 antibody in human cancer immunotherapy. *Curr Opin Immunol*. 2006;18(2):206–213.
70. Pulaski BA, Ostrand-Rosenberg S. Mouse 4T1 breast tumor model. *Curr Protoc Immunol*. 2001; 39(Chapter 20):Unit 20.2.1–20.2.16.
71. Lurquin C, et al. Contrasting frequencies of antitumor and anti-vaccine T cells in metastases of a melanoma patient vaccinated with a MAGE tumor antigen. *J Exp Med*. 2005;201(2):249–257.
72. Nam JS, et al. An anti-transforming growth factor beta antibody suppresses metastasis via cooperative effects on multiple cell compartments. *Cancer Res*. 2008;68(10):3835–3843.
73. Takaki R, et al. IL-21 enhances tumor rejection through a NKG2D-dependent mechanism. *J Immunol*. 2005;175(4):2167–2173.
74. Groh V, Bahram S, Bauer S, Herman A, Beauchamp M, Spies T. Cell stress-regulated human major histocompatibility complex class I gene expressed in gastrointestinal epithelium. *Proc Natl Acad Sci U S A*. 1996;93(22):12445–12450.
75. Hoos A, et al. Development of ipilimumab: contribution to a new paradigm for cancer immunotherapy. *Semin Oncol*. 2010;37(5):533–546.
76. Dewan MZ, et al. Fractionated but not single-dose radiotherapy induces an immune-mediated abscopal effect when combined with anti-CTLA-4 antibody. *Clin Cancer Res*. 2009;15(17):5379–5388.
77. Leach DR, Krummel MF, Allison JP. Enhancement of antitumor immunity by CTLA-4 blockade. *Science*. 1996;271(5256):1734–1736.
78. von Andrian UH. Intravital microscopy of the peripheral lymph node microcirculation in mice. *Microcirculation*. 1996;3(3):287–300.
79. Vijh S, Pilip IM, Pamer EG. Effect of antigen-processing efficiency on in vivo T cell response magnitudes. *J Immunol*. 1998;160(8):3971–3977.
80. Bromley SK, Peterson DA, Gunn MD, Dustin ML. Cutting edge: hierarchy of chemokine receptor and TCR signals regulating T cell migration and proliferation. *J Immunol*. 2000;165(1):15–19.

81. Champsaur M, Lanier LL. Effect of NKG2D ligand expression on host immune responses. *Immunol Rev*. 2010;235(1):267–285.
82. Lindquist RL, et al. Visualizing dendritic cell networks in vivo. *Nat Immunol*. 2004;5(12):1243–1250.
83. Hugues S, Fetler L, Bonifaz L, Helft J, Amblard F, Amigorena S. Distinct T cell dynamics in lymph nodes during the induction of tolerance and immunity. *Nat Immunol*. 2004;5(12):1235–1242.
84. Miller MJ, Wei SH, Parker I, Cahalan MD. Two-photon imaging of lymphocyte motility and antigen response in intact lymph node. *Science*. 2002; 296(5574):1869–1873.
85. Quezada SA, Peggs KS, Simpson TR, Shen Y, Littman DR, Allison JP. Limited tumor infiltration by activated T effector cells restricts the therapeutic activity of regulatory T cell depletion against established melanoma. *J Exp Med*. 2008;205(9):2125–2138.
86. Laird NM, Donnelly C, Ware JH. Longitudinal studies with continuous responses. *Stat Methods Med Res*. 1992;1(3):225–247.